Journal of Astronomical Telescopes, Instruments, and Systems

AstronomicalTelescopes.SPIEDigitalLibrary.org

High-energy proton radiation damage experiment on a hybrid CMOS detector

Evan Bray
Abraham D. Falcone
Mitchell Wages
David N. Burrows
Carl R. Brune
Zach Meisel

SPIE.

Evan Bray, Abraham D. Falcone, Mitchell Wages, David N. Burrows, Carl R. Brune, Zach Meisel, "High-energy proton radiation damage experiment on a hybrid CMOS detector," *J. Astron. Telesc. Instrum. Syst.* **6**(1), 016002 (2020), doi: 10.1117/1.JATIS.6.1.016002

High-energy proton radiation damage experiment on a hybrid CMOS detector

Evan Bray,[a,*] Abraham D. Falcone,[a] Mitchell Wages,[a] David N. Burrows,[a] Carl R. Brune,[b] and Zach Meisel[b]

[a]The Pennsylvania State University, Department of Astronomy and Astrophysics, University Park, Pennsylvania, United States

[b]Ohio University, Department of Physics and Astronomy, Athens, Ohio, United States

Abstract. We report on the results of an experiment to determine the effects of radiation damage caused by high-energy protons on an x-ray hybrid CMOS detector. This detector was utilized in a previous proton radiation experiment, which delivered a total dose to a selected region of ~3 krad (Si). With updated hardware and experimental procedures, we further irradiated the detector with 7-MeV protons, delivering an additional 1.5 krad (Si) (2.78×10^9 protons/cm^2 10 MeV equivalent) with increased uniformity to an overlapping region. The effects of this radiation on several important detector characteristics were analyzed after delivering doses of 0.5 and 1.0 krad. After 16 h of annealing at room temperature, detector performance was found to be unchanged in both cases. © *2020 Society of Photo-Optical Instrumentation Engineers (SPIE)* [DOI: 10.1117/1.JATIS.6.1.016002]

Keywords: x-rays; hybrid CMOS detectors; high-energy protons; radiation damage; displacement damage.

Paper 19086 received Aug. 20, 2019; accepted for publication Mar. 16, 2020; published online Mar. 31, 2020.

1 Introduction

To properly design and plan for future x-ray space telescopes, it is necessary to understand the long-term effects of operating a sensitive imaging device in a high-energy radiation environment. The precise effects of radiation damage on various solid-state imaging devices is a well-documented field, with many methodical studies and thorough simulations over the past several decades.[1–5] The relevant physics and damage mechanisms will not be discussed in-depth in this work, but a high-level overview can be found in Srour et al.[6] The interaction process being explored by this experiment is that of displacement damage in the silicon lattice. In orbit, this damage is typically caused by high-energy protons and electrons, and is the primary cause of performance degradation in space-based solid-state imaging arrays.[7] For a device in low-Earth orbit, the largest fraction of total damage comes from energetic protons (1 to 100 MeV) that are capable of penetrating through the detector shielding. Although the effects of radiation damage in silicon tend to follow a general trend, precise results are a strong function of device architecture.

Of particular interest are radiation damage studies performed on the current generation of x-ray telescopes, including the Chandra X-ray Observatory,[8–10] XMM-Newton,[11,12] and the Neil Gehrels Swift Observatory.[13,14] After the launch of Chandra, it was found that low-energy (~100 keV) protons were unexpectedly being focused by the x-ray optics into the focal plane of the instrument.[15,16] This led to a rapid increase in charge transfer inefficiency of the front-illuminated CCDs on board and motivated a change in procedure to translate the Advanced CCD Imaging Spectrometer (ACIS) out of the focal plane during passages of the Earth's radiation belts. By closely monitoring the performance of the devices in the focal plane of these instruments, we gain a better understanding of the practical consequences of radiation damage in space telescopes. This knowledge can then be used to perform ground-based experiments that will

*Address all correspondence to Evan Bray, E-mail: Bray.EvanP@gmail.com

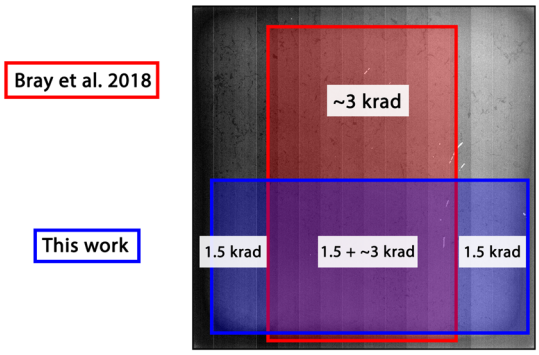

Fig. 1 A single frame taken by H1RG-161, with the regions damaged by proton radiation overlaid.

more accurately reflect the characteristics of a detector in orbit. While a satellite's radiation environment can vary significantly depending on its orbital parameters, a common region of interest is that of low-Earth orbit, just below the radiation belts. For a telescope in this orbit, such as Hubble or Swift, 1.5 krad corresponds to ~9 years of cumulative radiation damage from high-energy protons.[17]

The detector used in this experiment is an engineering-grade HyViSI H1RG hybrid CMOS detector (HCD) fabricated by Teledyne Imaging Sensors, which we are characterizing for the purposes of x-ray astronomy. It comprises 1024×1024 pixels with an 18-μm pitch and a 100-μm-thick silicon absorber layer. Prior to this work, this detector was irradiated at the Edwards Accelerator Laboratory using a different technique and received a cumulative dose of 3 krad (Si). The results of this irradiation are described by Bray et al.[18] (hereafter paper 1), and the overlap in irradiated regions between works is shown in Fig. 1. To achieve a higher degree of radiation uniformity, the experimental procedure from paper 1 was improved upon in order to guarantee an even exposure of the device. Simultaneously, this work utilizes a different set of detector hardware and a more optimized set of data taking procedures to better determine detector characteristics. Recent progress in characterizing HCDs for x-ray astronomy applications is discussed in several recent papers.[19–23]

2 Experimental Setup

This experiment was performed at the Edwards Accelerator Laboratory, which is operated by the Department of Physics and Astronomy at Ohio University. The detector setup was mounted on a beam line at the tandem electrostatic accelerator, as shown in Fig. 2. Protons of 8 MeV were incident on a 25-μm-thick tungsten scattering foil. After Rutherford scattering at an angle of 60 deg, the proton beam is degraded to 7 MeV with an energy spread of 0.7%. A silicon detector used for calibration was placed at an angle of 168 deg (calibration detector 1 in Fig. 2), and a second silicon detector was placed at the position that would later be occupied by the HCD. Once the flux scaling relation was determined between these two devices, the second silicon detector was replaced with the HCD. Dosimetry at the location of the HCD could be determined by measuring the flux incident on calibration detector 1. The final absorbed dose was delivered at a rate of 0.25 krad/h and was controlled by facility staff. Total uncertainty in the proton flux arriving at the center of the irradiated region is calculated to be 2%.

The incident protons impart a fraction of their energy at many points along their travel path as they inelastically scatter off atoms in the silicon lattice of the detector. However, a majority of their energy (and hence, the displacement damage) is delivered immediately before the incident particles come to rest. This is known as the Bragg peak and is a property of ionizing radiation that is traveling through matter. For the 7-MeV protons used here, the stopping distance in silicon is 386 μm, which is located within the readout integrated circuit (ROIC) layer of this backside-illuminated detector. An illustration of this phenomenon is shown in Fig. 3.

During irradiation, the detector was masked with tungsten sheets, cooled to a temperature of 130 K, and left unbiased. Because the SIDECAR used in this setup is a cryogenic model,

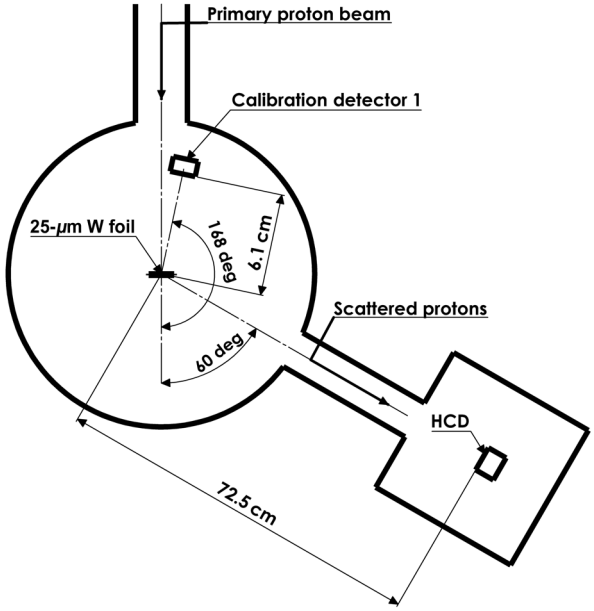

Fig. 2 A schematic representation of the experimental setup used for exposing the detector to high-energy protons via Rutherford scattering. The HCD was located at 60 deg to the beam axis, and a separate Si detector used for calibrating the required exposure length was located close to the tungsten foil at an angle of 168 deg.

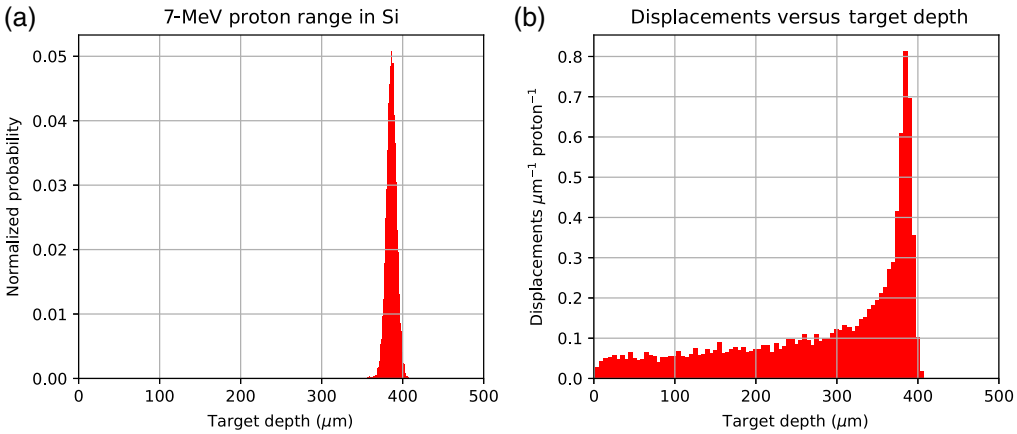

Fig. 3 Two plots generated using SRIM-2008[24] showing (a) stopping range and (b) displacement damage events per unit travel distance for 7-MeV protons in silicon.

the detector must be cooled to this level in order for the SIDECAR to reach its operating temperature of 180 K through a longer thermal path. Previous hardware setups that did not utilize a cryogenic SIDECAR showed detector performance that did not change appreciably between operation at 150 versus 130 K. After the radiation was delivered, the detector was allowed to warm up overnight before being cooled the following day to begin postirradiation characterization.

3 Postirradiation Characterization

The detector was irradiated with the methods described in Sec. 2 on two separate visits, separated about one month. The first visit delivered 0.5 krad, while the second delivered an additional 1 krad. In both cases, detector performance was characterized at several epochs after irradiation. The properties that were examined in this fashion include read noise (Sec. 3.1), dark current (Sec. 3.2), gain, and energy resolution (Sec. 3.3). Our results show that, after ∼16 h at room temperature, detector characteristics have returned to preirradiation levels after both doses.

After the radiation is delivered, detector characteristics are expected to change over time through a process called "annealing." This is the result of the mobile vacancies and defects produced in the silicon lattice reorganizing themselves into less harmful and more stable configurations. This process is highly temperature dependent and is often aided by baking out the detector at temperatures as high as 100°C. The effectiveness and potential of annealing during space missions is still a subject of ongoing study and is strongly dependent on detector architecture and fine details of the spacecraft design. One well-known example is the case of ACIS on board Chandra, where overall instrument performance was found to decrease after annealing at 30°C for 8 h. The cause of this behavior is likely due to a combination of factors, including charge trap reorganization, secondary defect generation, and increasing contaminant outgassing and accumulation rates.[25,26] Because these factors can be difficult to predict, the most reliable way to determine how a particular instrument will respond to radiation and the subsequent annealing process is through direct experimentation.

3.1 *Read Noise*

Read noise is evaluated for each individual pixel by analyzing pixel values for a large sample of images. By calculating read noise in this way, we can identify regions of the detector that are intrinsically noisier than others, as well as determine which precise region of the detector was irradiated. Examples of this technique at several epochs are shown in Fig. 4. After a large initial shift, read noise gradually returned to preirradiation levels over the next 24 h. A histogram comparing the pre- and post-irradiation values is shown in Fig. 5.

3.2 *Dark Current*

We measured the dark current by performing nondestructive reads of the detector during a series of 1-h ramps. No x-ray source was on while the images were being collected, and the ramps are strung together end-to-end so that the accumulated dark signal can be distinguished from the noise floor. We then determine dark current for each individual pixel by performing a linear fit to the measured pixel values across the entire data run. Dark current images are shown in Fig. 6. Due to time requirements, it was not possible to obtain a measurement of dark current immediately after irradiation, and the soonest that was feasible was the following day.

Removal of cosmic rays is performed by flagging pixel values that exhibited a sudden large increase in signal between frames. These data, along with the values in the eight surrounding pixels, are then removed prior to performing linear fits. This allows a relatively accurate measurement to be obtained even for pixels that had a portion of their data spoiled by background radiation. After an overnight anneal at room temperature, dark current was found to be unchanged from preirradiation levels.

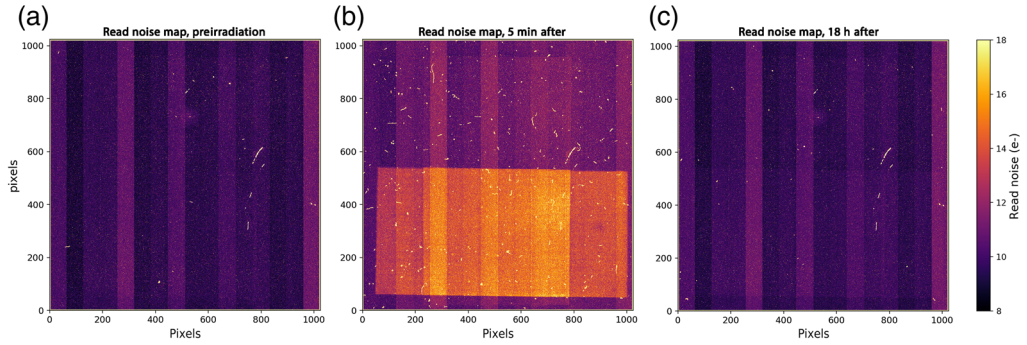

Fig. 4 A map of the read noise across the detector as measured at the Pennsylvania State University (PSU) (a) before receiving a 1-krad dose, (b) 5 min after receiving a 1-krad dose, and (c) 18 h after receiving a 1-krad dose, measured at Ohio University. A large initial shift can be seen immediately after irradiation, which then becomes increasingly faint over the course of the next 24 h. Differences between the 16 readout channels appear as vertical stripes in all images. It is worthy noting the increased number of background radiation events in the middle panel.

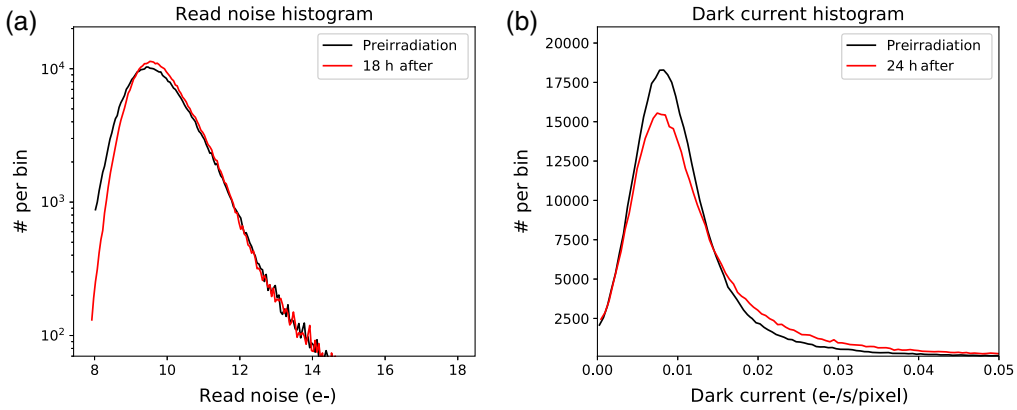

Fig. 5 Distribution of (a) read noise and (b) dark current values before and after receiving a 1-krad dose. Median values remain unchanged from preirradiation levels in both cases. Preirradiation curves were taken at PSU, while the postirradiation curves were obtained shortly after irradiation at Ohio University. The slightly elevated tail on the dark current histogram is likely due to the increased background radiation present at the radiation facility and its imperfect removal in the data analysis.

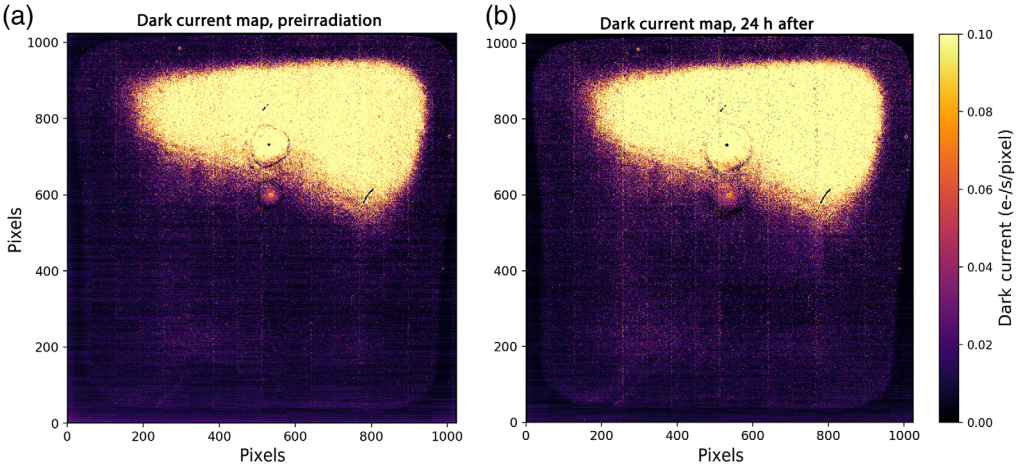

Fig. 6 A map of the dark current across the detector as measured (a) before receiving a 1-krad dose and (b) 24 h after receiving a 1-krad dose. The irradiated region on the bottom half of the detector remains unchanged from its preirradiation levels. The bright region in the top half of the detector is a voltage-dependent defect that leads to higher dark current in a localized area for this particular engineering-grade detector and is not caused by radiation damage.

3.3 *Energy Resolution*

Detector gain and energy resolution were measured by mounting an ^{55}Fe source on a movable shutter inside the vacuum chamber which allowed the source to be moved in and out of the detector field of view. Immediately after irradiation, a distinct shift in the digital number (DN) value of the centroid peak was observed. We believe that this is due to an actual shift in the gain of the readout amplifiers in the ROIC, as opposed to a decrease in the number of electrons that are produced by each x-ray that is reaching the collection node, due to a lack of "trailing charge" seen in event pixels during subsequent frames. After being allowed to warm to room temperature overnight, the energy resolution was found not to be significantly degraded from its preirradiation value. Because the H1RG architecture exhibits a significant amount of interpixel capacitance (IPC), the energy resolution of this detector at 5.9 keV is limited to ~7.5%. It should be noted that the problem of IPC has been solved in new generations of HCDs by utilizing capacitive trans-impedance amplifiers in the ROIC design, and that x-ray HCDs have achieved an energy resolution as low as 2.5% at 5.9 keV.[23,27]

Table 1 A summary of detector characteristics before and after the radiation dose described in this work. Additional cumulative dose refers to the dose of radiation that was applied to the lower half of the detector, as shown in Fig. 1. A portion of that region had received an earlier dose of ~3 krad.

Additional cumulative dose (krad)	Read noise (e^-)		Dark current (e^-/s/pixel)		Gain (DN/e^-)	$\Delta E/E$ at 5.9 keV (%)
	Median	SD[a]	Median	SD[a]		
0	9.68 ± 0.02	2.06	0.009 ± 0.001[b]	0.010	0.588	7.5
0.5 (after 24 h)	9.65 ± 0.02	2.14	0.009 ± 0.001[b]	0.008	0.594	7.6
1.5 (after 24 h)	9.71 ± 0.02	2.13	0.009 ± 0.001[b]	0.011	0.585	7.6

[a]Denotes standard deviation of the population of pixels within the irradiated region.
[b]Total uncertainty is dominated by systematic uncertainty due temperature control of the test stand.

4 Conclusion

After analyzing the data taken both pre- and post-irradiation, our findings show results that are consistent with previous experiments on similar devices. Specifically, the detector shows an initial degradation of read noise, dark current, and gain, followed by a slow annealing process that occurs on the timescale of ~12 h. After being warmed to room temperature overnight, no measurable amount of performance degradation was realized in read noise, dark current, gain, or energy resolution. These results are summarized in Table 1 and appear to indicate that only a modest level of annealing is necessary to preserve performance characteristics of detector. By continuing to test new generations of detectors using the methods described here, we can determine the extent to which x-ray HCDs can reliably operate in a space-like environment to meet the science goals of future large-scale missions.

Acknowledgments

We would like to thank the staff of the Physics Department at Ohio University and the Edwards Accelerator Lab for the generous use of their facilities and equipment, as well as providing the expertise and guidance necessary to ensure a smooth and successful experiment. This work was supported by the National Aeronautics and Space Administration under Grant Nos. NNX16AO90H and 80NSSC18K0147. The work at the Edwards Accelerator Laboratory was supported in part by the Ohio University College of Arts and Sciences and the U.S. Department of Energy under Grant No. DE-FG02-88ER40387. This paper has also been submitted to SPIE Proceedings.

References

1. C. Virmontois et al., "Total ionizing dose versus displacement damage dose induced dark current random telegraph signals in CMOS image sensors," *IEEE Trans. Nucl. Sci.* **58**(6), 3085–3094 (2011).
2. G. R. Hopkinson, "Radiation effects on CCDs for spaceborne acquisition and tracking applications," in *First Eur. Conf. Radiat. and Its Effects Devices and Syst.*, pp. 368–372 (1991).
3. N. Bassler, "Radiation damage in charge-coupled devices," *Radiat. Environ. Biophys.* **49**, 373–378 (2010).
4. G. R. Hopkinson, "Radiation effects in a CMOS active pixel sensor," *IEEE Trans. Nucl. Sci.* **47**(6), 2480–2484 (2000).
5. G. R. Hopkinson, C. J. Dale, and P. W. Marshall, "Proton effects in charge-coupled devices," *IEEE Trans. Nucl. Sci.* **43**(2), 614–627 (1996).
6. J. R. Srour, C. J. Marshall, and P. W. Marshall, "Review of displacement damage effects in silicon devices," *IEEE Trans. Nucl. Sci.* **50**(3), 653–670 (2003).

7. J. Janesick, T. Elliott, and F. Pool, "Radiation damage in scientific charge-coupled devices," *IEEE Trans. Nucl. Sci.* **36**(1), 572–578 (1989).
8. G. Y. Prigozhin et al., "Characterization of the radiation damage in the Chandra x-ray CCDs," *Proc. SPIE* **4140**, 123–134 (2000).
9. D. H. Lo and J. R. Srour, "Modeling of proton-induced CCD degradation in the Chandra X-ray Observatory," *IEEE Trans. Nucl. Sci.* **50**(6), 2018–2023 (2003).
10. C. E. Grant et al., "Long-term trends in radiation damage of Chandra x-ray CCDs," *Proc. SPIE* **5898**, 58980Q (2005).
11. E. Kendziorra et al., "Effect of low-energy protons on the performance of the EPIC pn-CCD detector on XMM-Newton," *Proc. SPIE* **4140**, 32–41 (2000).
12. L. Strüder et al., "pnCCDs on XMM-Newton—42 months in orbit," *Nucl. Instrum. Methods Phys. Res. Sect. A* **512**(1), 386–400 (2003).
13. A. D. Short, "SWIFT XRT: proton environment and CCD degradation," Swift project document: SWIFT-LUX-RE-001/1 (2000).
14. C. Pagani et al., "Recovering swift-XRT energy resolution through CCD charge trap mapping," *Astron. Astrophys.* **534**, A20 (2011).
15. B. Altieri, "Impact of space environment on x-ray satellite observatories: soft-protons clouds in the Earth magnetosphere," Space Studies Program, International Space University (2003).
16. B. K. Dichter and S. Woolf, "Grazing angle proton scattering: effects on Chandra and XMM-Newton x-ray telescopes," *IEEE Trans. Nucl. Sci.* **50**, 2292–2295 (2003).
17. R. M. Ambrosi et al., "The effect of proton damage on the x-ray spectral response of MOS CCDs for the SWIFT X-ray Telescope," *Nucl. Instrum. Methods Phys. Res. Sect. A* **482**(3), 644–652 (2002).
18. E. Bray et al., "Proton radiation damage experiment on a hybrid CMOS detector," *Proc. SPIE* **10709**, 107090L (2018).
19. S. V. Hull et al., "Recent x-ray hybrid CMOS detector developments and measurements," *Proc. SPIE* **10397**, 1039704 (2017).
20. S. V. Hull et al., "Small pixel hybrid CMOS x-ray detectors," *Proc. SPIE* **10709**, 107090E (2018).
21. E. Bray et al., "Exploring fine subpixel spatial resolution of hybrid CMOS detectors," *Proc. SPIE* **10699**, 106995Q (2018).
22. E. Bray et al., "Characterizing subpixel spatial resolution of a hybrid CMOS detector," *J. Astron. Telesc. Instrum. Syst.* **4**(3), 038002 (2018).
23. S. V. Hull et al., "Hybrid CMOS detectors for the Lynx x-ray surveyor high definition x-ray imager," *J. Astron. Telesc. Instrum. Syst.* **5**(2), 021018 (2019).
24. J. F. Ziegler, "Stopping range of ions in matter (SRIM)," http://www.srim.org/ (2008).
25. C. E. Grant et al., "Physics of reverse annealing in high-resistivity Chandra ACIS CCDs," *Proc. SPIE* **7021**, 702119 (2008).
26. S. L. O'Dell et al., "Modeling contamination migration on the Chandra X-ray Observatory IV," *Proc. SPIE* **10397**, 103970C (2017).
27. C. V. Griffith et al., "Speedster-EXD: a new event-driven hybrid CMOS x-ray detector," *J. Astron. Telesc. Instrum. Syst.* **2**(1), 016001 (2016).

Evan Bray is a recent graduate from the Department of Astronomy and Astrophysics at the Pennsylvania State University. His PhD research is focused on the characterization of x-ray hybrid CMOS detectors (HCDs) for the purposes of next-generation x-ray space telescopes. Currently, he is a member of the Environmental Test and Integration Services group at the Goddard Space Flight Center.

Abraham D. Falcone is a research professor of astronomy and astrophysics at the Pennsylvania State University. He received his BS degree in physics from Virginia Tech in 1995 and PhD in physics from the University of New Hampshire in 2001. He has authored more than 200 refereed journal publications. He leads research in fields ranging from x-ray and gamma-ray instrumentation to the study of particle acceleration at high-energy astrophysical sites, such as active galactic nuclei, gamma-ray bursts, and x-ray binaries.

David N. Burrows is a professor of astronomy and astrophysics at the Pennsylvania State University, where he has been involved in x-ray detector development, sounding rocket observations, and research on supernova remnants and gamma-ray bursts. He has coauthored over 300 refereed publications, and was awarded the 2007 Bruno Rossi Prize and the 2009 Muhlmann Award as a member of the Swift team, for which he leads the XRT team.

Biographies of the other authors are not available.